



Highly compact and cost-effective 2-beam super-resolution structured illumination microscope based on all-fiber optic components

JAKUB POSPÍŠIL,^{1,2} GERD WIEBUSCH,¹ KAREL FLIEGEL,² MILOŠ KLÍMA,² AND THOMAS HUSER^{1,*} 

¹*Biomolecular Photonics, Faculty of Physics, Bielefeld University, Bielefeld, Germany*

²*Department of Radioelectronics, Faculty of Electrical Engineering, Czech Technical University in Prague, Prague, Czech Republic*

**thomas.huser@physik.uni-bielefeld.de*

Abstract: Current super-resolution structured illumination microscopes (SR-SIM) utilize relatively expensive electro-optic components and free-space optics, resulting in large setups. Moreover, high power laser sources are required to compensate for the losses associated with generating the illumination pattern by diffractive optics. Here, we present a highly compact and flexible 2D SR-SIM microscope based on all-fiber optic components (fiberSIM). Fiber-splitters deliver the laser light to the sample resulting in the interference illumination pattern. A microelectromechanical systems (MEMS) based fiber switch performs rapid pattern rotation. The pattern phase shift is achieved by the spatial displacement of one arm of the fiber interferometer using a piezoelectric crystal. Compared with existing methods, fiberSIM is highly compact and significantly reduces the SR-SIM component cost while achieving comparable results, thus providing a route to making SR-SIM technology accessible to even more laboratories in the life sciences.

© 2021 Optical Society of America under the terms of the [OSA Open Access Publishing Agreement](#)

1. Introduction

Super-resolution structured illumination microscopy (SR-SIM) is one of the most attractive means of achieving a spatial resolution beyond the diffraction limit with fluorescence microscopy. SR-SIM typically doubles the spatial resolution of optical microscopy, which is readily sufficient to visualize cellular organelles and their substructures well below 200 nm [1–5]. In addition to this, SR-SIM is a widefield imaging method, making it highly efficient in the use of the available photon budget, while minimizing photoinduced effects which can be detrimental to sample health. This technique has been demonstrated to be able to image individual cells rapidly, over extended periods of time, and in multiple color channels, simultaneously. Even high speed implementations utilizing real-time image reconstruction have recently been realized, allowing biologists to readily explore living cells and their dynamics at super-resolution even during data acquisition.

Current implementations of SR-SIM devices are, however, rather bulky systems. They utilize relatively expensive opto-electronic components and diffractive optics, and their imaging speed is limited by the laser power available at the sample location. In SR-SIM systems based on diffraction optics only a fraction of the original laser light is delivered to the sample. This can e.g. limit high speed image acquisition because fluorescence might not be excited efficiently enough to result in sufficient signal strength at low exposure times. Moreover, the rate at which some electro-optic devices, such as liquid crystal-based spatial light modulators [5–7], can switch between patterns is typically also limiting the overall imaging rate.

Currently, most 2D and 3D SR-SIM realizations are based upon utilizing the interference pattern generated by projecting the $\pm 1^{\text{st}}$ and 0^{st} (in the 3D case) diffraction orders of a diffraction

grating to the focal plane of a fluorescence microscope. 2-beam interference patterns are typically utilized to achieve 2D resolution enhancement in the lateral direction, while 3-beam interference patterns allow for 3D resolution enhancement [2,4]. If one, however, reminds oneself that SR-SIM is based on exciting fluorescence by interference fringes, then other means of creating and rapidly changing such patterns can be envisioned. Alternative ways of creating stable interference patterns, e.g. by laser beam interferometry, could also be devised and have been used in the past. E.g. Frohn et al. used interfering waves along the x- and y-direction created by deflecting laser beams at high incidence angles via a prism-system to the focus plane of an inverted microscope to realize one of the first SIM systems [8], which was followed by Brunstein and coworkers, who utilized a compact Michelson-type interferometer to achieve total internal reflection fluorescence excitation SIM (TIRF-SIM) along three lateral directions [9]. Similarly, Cnossen et al. used an interferometric 2-beam SIM system to demonstrate a factor of 2 improvement in the localization of single fluorescent molecules in a mechanism they called “SIMFLUX” [10,11]. While optical fiber-based interferometers have, however, been utilized extensively to set up optical coherence tomography (OCT) instruments [12,13], they are currently underrepresented in SR-SIM microscopy, although such systems can offer some significant advantages. A particular advantage of fiber-based interferometry is the significantly lower loss in excitation light, which is limited to the amount of light that can be coupled into a single-mode fiber. Just this advantage alone would allow one to readily set up SR-SIM systems with less expensive low power lasers. In addition, optical fibers readily provide high stability, and, thus, robustness, to interferometers. They also allow for easy and very flexible means of light delivery. Already in 2006, Chung et al. used fiber-delivered laser beams to set up an objective-type TIRF-SIM system [14], while more recently, Chang et al. used fiber-delivered 2-beam interferometry to create a SIM-type interference pattern in opposing light sheets [15].

Here, we detail the development and operation of a SR-SIM microscope based on all-fiber optic components and we demonstrate its imaging performance. Single-mode fiber-optic 1×2 splitters are used to set up coherent light paths to generate 2D interference patterns at specific illumination angles. A microelectromechanical systems (MEMS) based fiber switch is used to rapidly switch between different illumination angles, while the piezoelectric crystal-controlled displacement of fiber collimators provides the phase shifting required for 2D SR-SIM image reconstruction. This results in extremely flexible, compact, and robust SR-SIM illumination optics. We demonstrate and analyze its ability to efficiently generate SR-SIM illumination patterns. We also demonstrate the performance of this system by imaging mono-layers of fluorescent beads and by analyzing the resulting images using global metrics for determining image resolution.

2. Results

In this section, a detailed description of the fiberSIM setup as well as the results of an SR-SIM image acquisition and reconstruction experiment are provided.

2.1. Optical system

To realize our SR-SIM setup based on all-fiber optic components, a diode-pumped solid state laser operating at a wavelength of 532 nm and a power of 30 mW is coupled into the input fiber of a 1×4 microelectromechanical systems (MEMS) single-mode fiber switch (Sercalo AG, Switzerland). This device is designed for highly reliable and rapid switching between 4 different output fibers. (Details about the actual switching speed of the device are discussed in the section *Performance of illumination angle switching using a MEMS switch*). Three of these output fibers are used for the SR-SIM system to select between the three different angles under which the interference pattern is generated. Each one of the output fibers is connected to a 1×2 fiber splitter (Thorlabs, Inc., USA) and the ends of these fibers are then used to define a specific angle of illumination. Since the current implementation does not (yet) utilize polarization maintaining

fibers, in-line fiber polarization controllers (Thorlabs, Inc., USA) are utilized to adjust the output polarization state and, thus, to control the output power of each fiber. (Details are discussed in the *Discussion* section). The two branches of the 1×2 fiber splitter are placed opposite each other to form a pair (see Fig. 1), and each pair position is rotated by 60° with respect to each other. In total, six fiber outputs are mounted in a custom-made hexagonal fiber holder comprised of 6 collimation units housing a single lens for each fiber ($L1_a$ - $L1_f$: $f = 25$ mm).

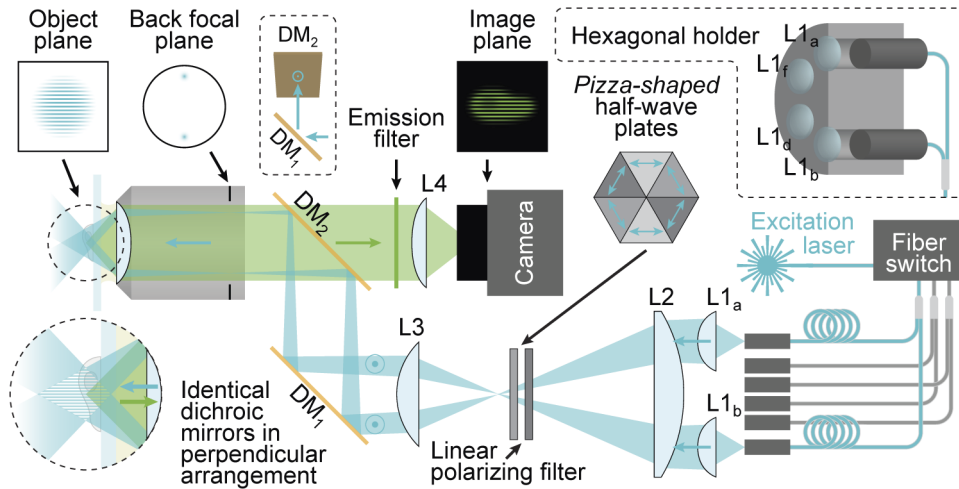


Fig. 1. Schematics of the fiberSIM system. A hexagonal holder holds 6 fiber collimators in 60° intervals. A combination of two fiber collimators ($L1_a$, and $L1_b$) with a relative displacement of 180° are placed in equal distance from the central axis of the hexagonal holder. Each one of these two collimators focus a laser beam to the back focal plane of a 60×/1.45NA objective lens (Olympus, Japan), resulting in a striped interference pattern at the object plane of the objective lens. Three pairs of the fiber collimators define the respective angles of illumination for the interference pattern. Lenses L2 and L3 form a telescope that changes the separation between two beams of each pair to accommodate the back focal plane of the objective lens. The polarization of each beam is rotated by *pizza-shaped* half-wave plates in between lenses L2 and L3. A pair of identical dichroic mirrors in the perpendicular arrangement ensures that the polarization state of the excitation light is maintained. Rapid switching between pattern angles is performed by the fast MEMS fiber switch. Displacement along the axial direction of one collimator in a pair results in phase shifting of the illumination pattern in the object plane. Fluorescence emission is captured by the same objective lens and lens L4 focuses the fluorescence light to the CMOS camera chip.

Figure 1 shows an illustration of the all-fiber optic SR-SIM setup. Outfitting each fiber with its own individual collimating lens creates flexibility for focusing patterns with different opening angles to the back focal plane of the objective lens. This allows for free placement of the collimating holder relative to the microscope objective lens, enabling one to easily switch objective lenses based on the specific application. The physical dimensions of the collimating lenses set the minimum separation between the adjacent parallel beam pairs to 33 mm. The diameter of the back focal plane of the objective lens (Olympus, Japan) is ~ 10 mm. Therefore, the separation between the beams is varied with a telescope (lenses L2: $f = 300$ mm, and L3: $f = 50$ mm). Suitable selection of telescope lenses, and thus the separation between the beams, allows us to easily change and adapt the pattern frequency of the 2-beam SIM microscope. The polarization state for each beam pair is rotated by placing a linear polarizing filter and a *pizza-shaped* half-wave plate (Bolder Vision Optics, USA) between the telescope lenses. To

separate the excitation light from the fluorescence signal and maintain the polarization of the excitation light, a pair of identical dichroic mirrors in the perpendicular arrangement is used [16,17]. In the perpendicular arrangement the dichroic mirrors are placed such that the first one reflects light within the plane of the optical table, while the second one reflects light upwards (perpendicular to the optical table). Fluorescence emission from the sample is collected by the same objective lens and the tube lens (L4: $f = 200$ mm) focuses the light to a CMOS camera chip. In this setup, an inexpensive industry-grade CMOS camera (IDS, Germany) acquires the raw SIM images with a frame rate up to 41 fps. Photographs of the setup as well as the individual components are shown in Fig. 2. The theoretical line spacing of the interference pattern λ' can

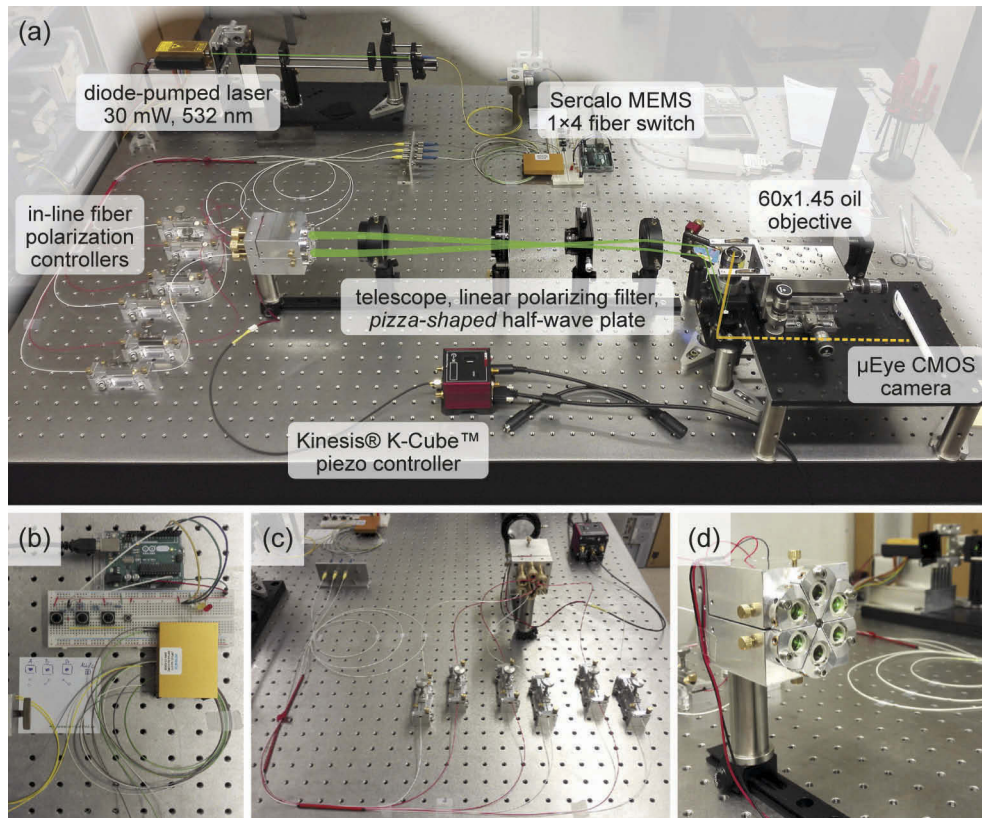


Fig. 2. Photo of the fiberSIM microscope. A diode-pumped solid state laser is coupled into the input fiber of a 1×4 MEMS fiber switch (b). Three output fibers are each connected to a 1×2 fiber splitter, respectively. The two fiber branches of each splitter are placed opposite each other to form a pair in the hexagonal holder (d). The polarization state in every one of the 6 single mode fibers is controlled individually by an in-line fiber polarization controller (c). Dedicated collimating lenses for each fiber focus the laser beams (green) to the back focal plane of the objective lens resulting in the interference pattern in the object plane. The separation between the beams is varied with a telescope. The power of each individual beam is also adjusted by the in-line fiber polarization controllers in combination with a linear polarizing filter. The final polarization state for each beam pair is rotated by a *pizza-shaped* half-wave plate placed after the linear polarizing filter. Fluorescence emission from a sample (yellow) is collected by the same objective lens and the tube lens focuses the light to the CMOS camera chip (a tube lens and CMOS camera are placed underneath the black base plate).

be defined as

$$\lambda' = \frac{\lambda_{ex} \cdot f}{d} = \frac{532 \text{ nm} \cdot 3 \text{ mm}}{5.5 \text{ mm}} = 290 \text{ nm}, \quad (1)$$

where λ_{ex} is the wavelength of the excitation laser, d is the distance between the interfering beams at the back focal plane of the objective lens, and f is the objective lens' principal focal length. The actual spacing of the interference line pattern observed in our raw SIM data is 300 nm.

It should be noted that changes in the separation between the beams in the back focal plane of the microscope objective lens currently requires changing lens combinations in the telescope of our fiberSIM system. Thus, it is lacking the flexibility provided by the choices in patterns that can be projected by a SLM-based SIM system [18]. We are, however, currently developing methods that allow for the flexible adjustment of the separation of the beams in the back focal plane, which will enable us to easily switch to grazing incidence and even TIRF excitation, where the highest spatial resolution in linear SR-SIM is achieved. Another benefit of our fiber-based SR-SIM implementation is that in a multicolor laser excitation system the beam separation remains the same. Thus, incidence angles are maintained, which is rather important for TIRF and grazing incidence SR-SIM, and this makes such implementations more straight-forward.

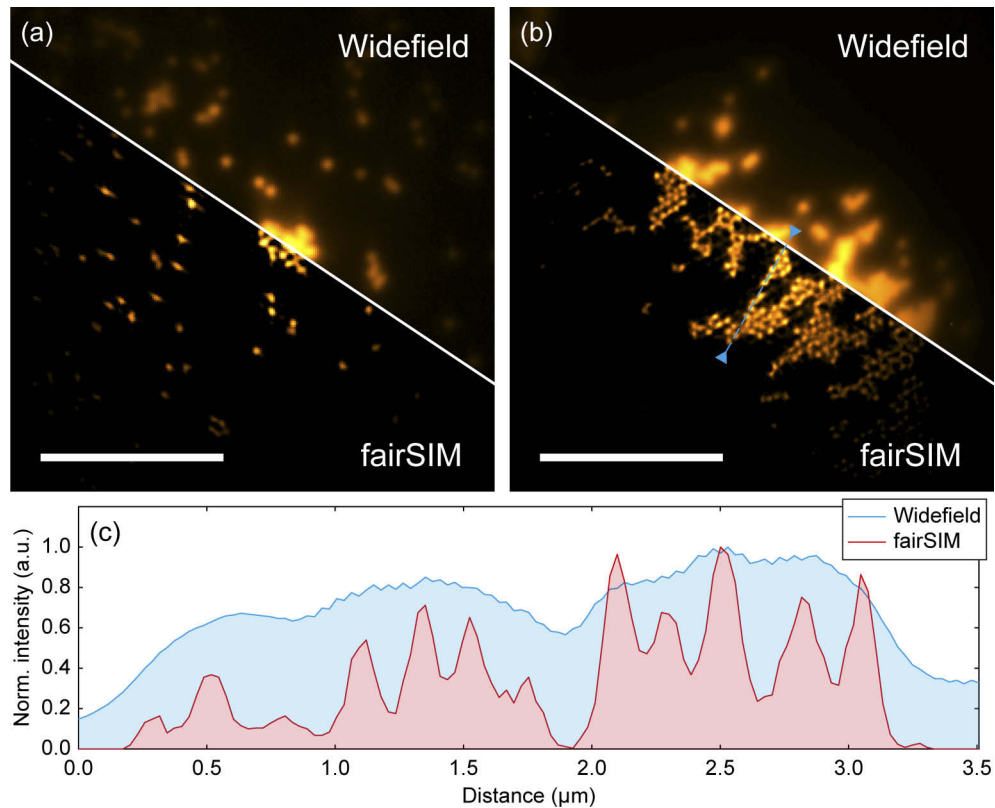


Fig. 3. Reconstructed super-resolution structured illumination microscopy (SR-SIM) images of 200 nm diameter fluorescent beads. Both images ((a) and (b)) show a field of view of $13.25 \mu\text{m} \times 13.25 \mu\text{m}$ of the single layer of 200 nm fluorescent beads. The resolution improvement can be seen in the lower diagonal of each image, resulting in the individual beads becoming distinguishable after SR-SIM reconstruction. (c) The resolution and contrast improvement along the line profile indicated in image (b) by a blue dashed line with arrows. Scale bars are $5 \mu\text{m}$.

2.2. SR-SIM imaging results

To demonstrate the imaging performance of our compact all-fiber optic SR-SIM microscope, a sample consisting of a mono-layer of TetraSpeck fluorescent beads with a diameter of 200 nm was prepared. SR-SIM image reconstruction was performed by using two open-source tools. The ImageJ and Fiji plugin fairSIM (<https://www.fairsim.org>) [19] uses the standard Gustafsson super-resolution SIM (SR-SIM) reconstruction method [1,3], while the MATLAB modular set of functions contained in SIMToolbox (<https://simtoolbox.github.io>) [20,21] utilizes maximum a posteriori probability SIM (MAP-SIM) [20] image reconstruction. Widefield images were generated by averaging all 9 raw diffraction-limited images into a single image. Figure 3 clearly shows the enhancement in lateral resolution and overall image contrast which can be obtained by our system. Figure 3(c) shows the line profiles of both the widefield and SR-SIM images, revealing the significant improvement in contrast. A detailed analysis and discussion of the system's performance by evaluating the lateral resolution gain is provided in the section *Spatial resolution achieved with all-fiber optic SR-SIM*.

3. Discussion

In the following section, we provide detailed descriptions of the all-fiber optic SR-SIM approach, including a discussion of the performance of the individual components and an analysis of the lateral resolution improvement achieved with this implementation.

3.1. Performance of illumination angle switching using a MEMS switch

The ultra-compact MEMS based 1×4 fiber switch (Sercalo AG, Switzerland) is utilizing non-polarization maintaining broadband single mode fibers in the wavelength range of 480 nm - 650 nm. It provides a fairly low cost, but high speed means of switching light from an input fiber to four output fibers. The switching time between the four different output fibers is ~ 3.5 ms (see Fig. 6(b)). Careful control of the polarization of interfering beams is critical for achieving a high pattern modulation depth. To control the polarization of the beams emitted from the non-polarization maintaining fibers, an in-line fiber polarization controller (Thorlabs, Inc., USA) is used for each optical fiber. These controllers in combination with the linear polarizing filter allow us to adjust the power of each individual beam. The *pizza-shaped* half-wave plate (Bolder Vision Optics, USA) placed directly after the linear polarizing filter set the correct polarization for each beam pair to maximize the interference modulation depth. Being able to adjust the power of each beam is especially useful to compensate the different coupling efficiencies of the different fiber switch outputs and the coupling ratio tolerance of the 1×2 fiber splitters. In order to ensure that the intensities of all 6 beams are set equally, a CMOS camera can be placed at the position of the back focal plane instead of the objective lens. Figure 4 shows an example of a measurement of the beam intensities before and after intensity adjustment with the in-line fiber polarization controllers.

3.2. Calibrating the phase-shifting accuracy of the illumination pattern

Shifting the phase of the interference pattern is achieved with a piezoelectric crystal (piezo). The piezo is a part of the hexagonal fiber collimator assembly, which is split in two opposing halves. One half, containing 3 fibers and their corresponding collimating lenses, can glide on metal rods in the direction of the laser beams and is pulled against the piezo by a spring. By applying a voltage to the piezo, the piezo translates this half of the assembly against the stationary other half, resulting in a defined path length difference (phase shift). In this initial implementation, we use an inexpensive piezoelectric crystal (Thorlabs, Inc., USA) operated in open-loop mode to achieve the spatial displacement of one of the fibers in each pair by up to 2 μm. Since the piezo does not contain a feedback sensor to monitor its length change, the corresponding phase change, and in

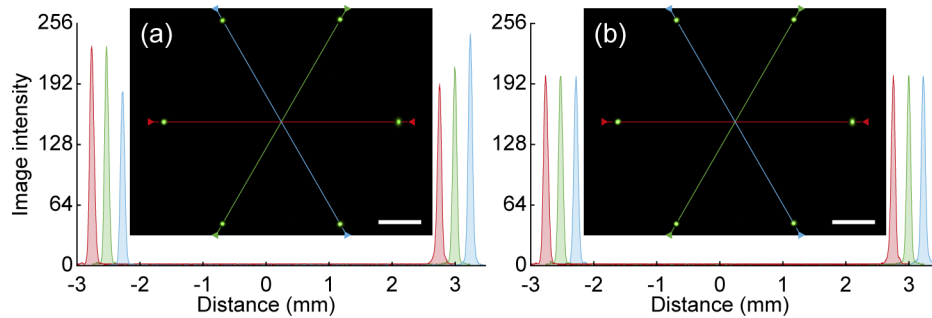


Fig. 4. Example of the intensity profiles of the individual laser beams focused to the back focal plane of the microscope objective lens before and after in-line fiber polarization controller based adjustments. (a) The image is the sum of three individual images (one image = one angle) where the intensities of the focus of each beam are not yet controlled. (b) The same image as shown in (a) after individual adjustment of the polarization state within each optical fiber by the in-line fiber polarization controller. The red, green and blue lines represent the line profiles taken for each angle in the image, at 0° , 60° , and 120° , respectively. Line profiles are shown shifted along the x-axis with a step size of $240\ \mu\text{m}$ to avoid overlapping of the peaks for better comparison. The field of view is limited by the physical size of the camera sensor ($7.093\ \text{mm} \times 5.320\ \text{mm}$), thus the line profiles are limited to 6 mm despite the diameter of the back focal plane of the objective lens being $\sim 10\ \text{mm}$. Scale bars are 1 mm.

particular its reproducibility, need to be calibrated a priori. Precise knowledge of the phase of the SR-SIM illumination pattern is a rather critical parameter for accurate image reconstruction. If the phase estimation, which is typically conducted by analyzing raw SR-SIM images [21–23], is not sufficiently precise, then artifacts, i.e. line breaks, are created during image reconstruction. Such artifacts can also occur if the phase estimation is conducted only once on an initial raw image set, and it is then assumed that the phase shift is reproducible for images acquired at a later time point. These artifacts can be avoided either by accurately determining the phase shift for every raw image individually or by ensuring a very high degree of reproducibility, e.g. by using a piezo with a capacitive feedback sensor. Here, we chose the first method, while also ensuring that the inexpensive piezo is operated in a highly linear range of the induced phase shifts. Figure 5 shows the dependence of the phase shift on the applied voltage of the piezo in the full range from 0 V to 150 V. To examine the reproducibility of the phase shift, the experiment was performed in 30 consecutive cycles, which are shown in Fig. 5(a). The mean of the 30 individual curves and the standard deviation shown in Fig. 5(b) illustrate the nonlinearity of the piezo displacement over the full voltage range. However, in the region from approximately 65 V to 120 V the curve is sufficiently linear in order to generate the equidistant phase shift over 2π as needed for successful artifact-free image reconstruction. The three dashed lines show the voltage points which were chosen for the three phase shifts required for successful SR-SIM image reconstruction. Please note that the displacements in the curves shown in Fig. 5(a) indicate a consistent unilateral long-term phase shift between the first and the last measurement of the cycle. This is currently the main source of uncertainty between the phase shifts. Improving the mechanical and thermal stiffness of the setup should allow us to further and drastically reduce this uncertainty.

3.3. Performance of the hexagonal fiber collimator

To examine the speed of our SR-SIM system, two experiments were performed. The time that it takes for the MEMS fiber switch to switch between output fibers (controlling the illumination pattern rotation) and the time that it takes the piezo-electric element to shift between discrete

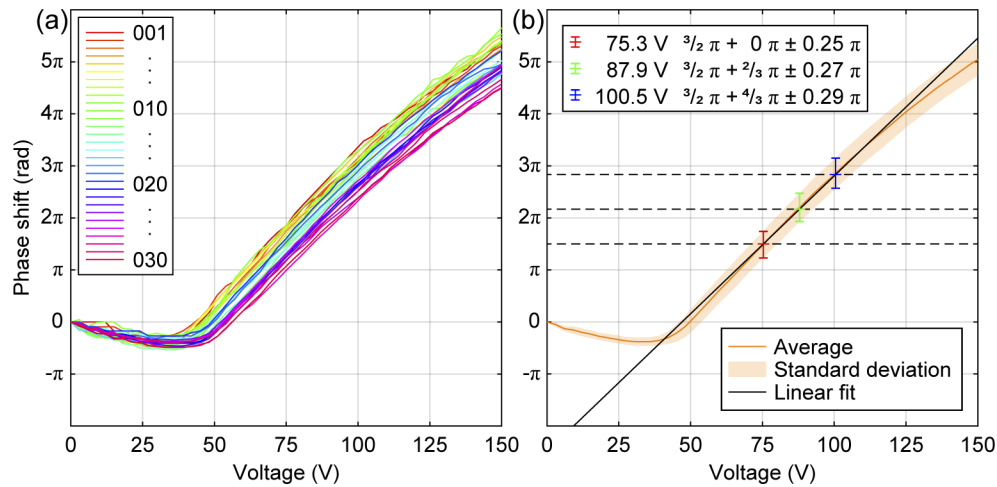


Fig. 5. Measurement of the interference pattern phase shift induced by open-loop piezoelectric displacement of the fiber collimators. The graphs show a dependence of the pattern phase on the voltage applied to the piezoelectric crystal. (a) The phase curves were obtained by conducting the experiment in 30 cycles by applying a voltage between 0 V to 150 V with a step size of 2 V to the piezo crystal. (b) The mean (orange line) and the standard deviation (light orange area) of the measurements. The linear regression (black line) fits the average data in the range between 65 V to 120 V where the average phase shift exhibits an almost linear dependence on voltage. Black dashed lines indicate the ideal phase shifts of patterns (with $3\pi/2$ offset) utilized for the subsequent SR-SIM image reconstruction. The standard deviation of each phase shift is indicated by a colored error bar (red, green, and blue). This step size is equal to $2\pi/3$ to cover the entire field of view with 3 phase steps.

phase settings were measured. A free-space biased photo detector (Si detector DET10A, Thorlabs, Inc., USA) in combination with a digital oscilloscope was used for detecting the incidence light of the fiber collimators. The oscilloscope input is equipped with a load resistor $R_{load} = 1 \text{ M}\Omega$ and the photo detector has a junction capacitance $C_j = 6 \text{ pF}$. This configuration leads to the photo detector time response t_r equal to $13.2 \mu\text{s}$ which is sufficient for our measurements as can be seen below.

The time response between *OFF* and *ON* states of the fiber switch (see Fig. 6(b)) was measured by placing the photo detector directly in front of one of the six output collimators. For the measurement of the phase shifting speed, one pair of fiber collimator lenses focuses the beams to the negative focal plane of a $f = 1000 \text{ mm}$ lens. This creates a coarse interference pattern (line spacing of $125 \mu\text{m}$) in the positive focal plane where the photo detector with a pinhole of diameter $20 \mu\text{m}$ is placed. This configuration allows us to sample the sinusoidal pattern with 6.25 samples over 2π . To ensure the maximum intensity difference on the photo detector, a phase shift of 1π resulting in a change from maximum intensity to a local minimum of the sinusoidal pattern. The smaller phase step of $2\pi/3$ as required for the pattern displacement in SR-SIM will, thus, only be faster.

If we consider that 3 angles in conjunction with 3 phase shifts per angle are required to reconstruct a 2D SR-SIM image, then the time required for switching these 9 patterns is equal to 39 ms. This corresponds to 3 phase shifts ($3 \times 6 \text{ ms}$) and 6 switches of the angle ($6 \times 3.5 \text{ ms}$) - 3 remaining angle switches are executed simultaneously with the phase shift (see Fig. 6(c)). The theoretical maximum SR-SIM image rate can then reach $\sim 26 \text{ fps}$. The inexpensive industrial CMOS camera (IDS, Germany) which we utilized can run at a rate of up to 41 fps. An acquisition of 9 consecutive images reduces the actual frame rate down to $\sim 4.5 \text{ fps}$, which makes the camera

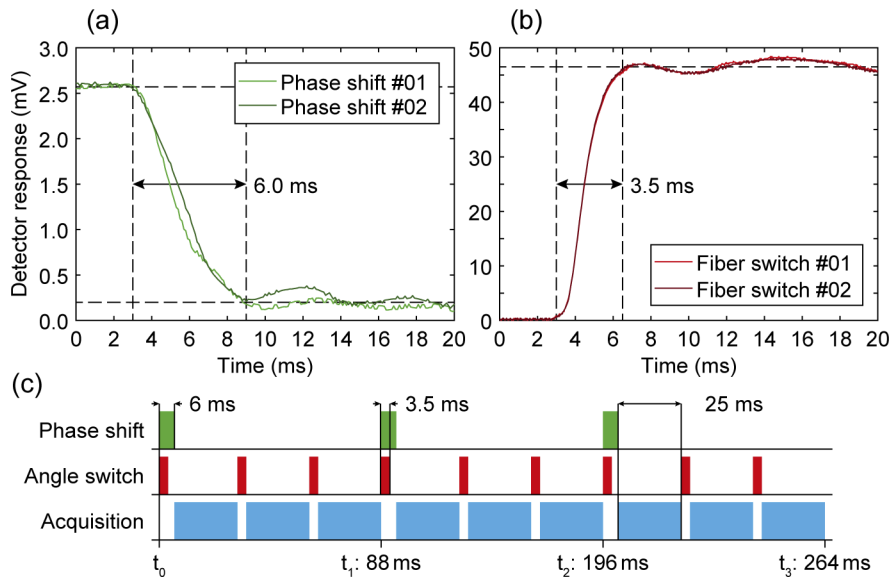


Fig. 6. Speed measurements of the electro-mechanical components in the setup and timing diagram of the current SR-SIM raw data acquisition. (a) Measurement of the time required for a phase shift of 1π , where the horizontal dashed lines represent the maximum and minimum photo detector response, thus the maximum and minimum intensities of the sinusoidal line pattern. (b) Measurement of the time required for the MEMS fiber switch to switch from *OFF* to *ON* state. In both graphs negligible ringing can be observed. (c) Timing diagram representing an acquisition of one raw dataset of 9 images (3 angles \times 3 phases) required for 2D SR-SIM reconstruction.

image acquisition time (~ 25 ms) the only speed limitation of the fiber-based SR-SIM illumination unit. The current setup can run up to ~ 4 SR images per second. If sliding window reconstruction is utilized [24], then this frame rate increases to ~ 34 fps. Currently, the relatively long distance between the hexagonal collimator and the objective lens, as required by the long telescope ($f_{L2} + f_{L3} = 350$ mm), in combination with the telescope's magnification ($f_{L2}/f_{L3} = 6\times$), results in a very narrow cone of the laser beam focused to the back focal plane, and thus restricts the effective field of view (FOV) of the illumination unit to $\sim 10\ \mu\text{m}$. This unit is, however, designed for flexibility, so that a larger FOV can be achieved by utilizing different lens sets.

3.4. Spatial resolution achieved with all-fiber optic SR-SIM

We determined the SR-SIM improvement of the spatial resolution by two automated methods used to assess the resolution of a single fluorescence microscope image. In both approaches, i.e. power spectral density analysis (PSD_{ca}) [25,26], and image decorrelation analysis [27], the maximum spatial frequency where the signal still contains useful information is determined.

Figure 7 shows the results of assessing the spatial resolution of the individual widefield and SR-SIM images. From the images in Fig. 7(a)–7(c) it can be seen that the spatial resolution improvement is sufficient to distinguish individual fluorescent beads in the SR-SIM reconstructed images (7(b) and 7(c)). Although samples of fluorescent beads with a diameter of 200 nm were analyzed, SR images can contain smaller details (higher frequencies in the Fourier transform), e.g. sharp edges of each bead or a group of beads. Therefore, two global metrics assessing the resolution of the entire image were used. Results of assessing the resolution by PSD_{ca} and decorrelation analysis are demonstrated in Fig. 7(e)–7(f). Image 7(d) shows sections of the Fourier transform of the widefield, MAP-SIM, and fairSIM images (7(a)–7(c)), respectively.

Dashed lines correspond to the cut-off frequencies determined by the PSD_{ca} method. Both measurements show a resolution improvement by almost a factor of 2 in both super-resolved images.

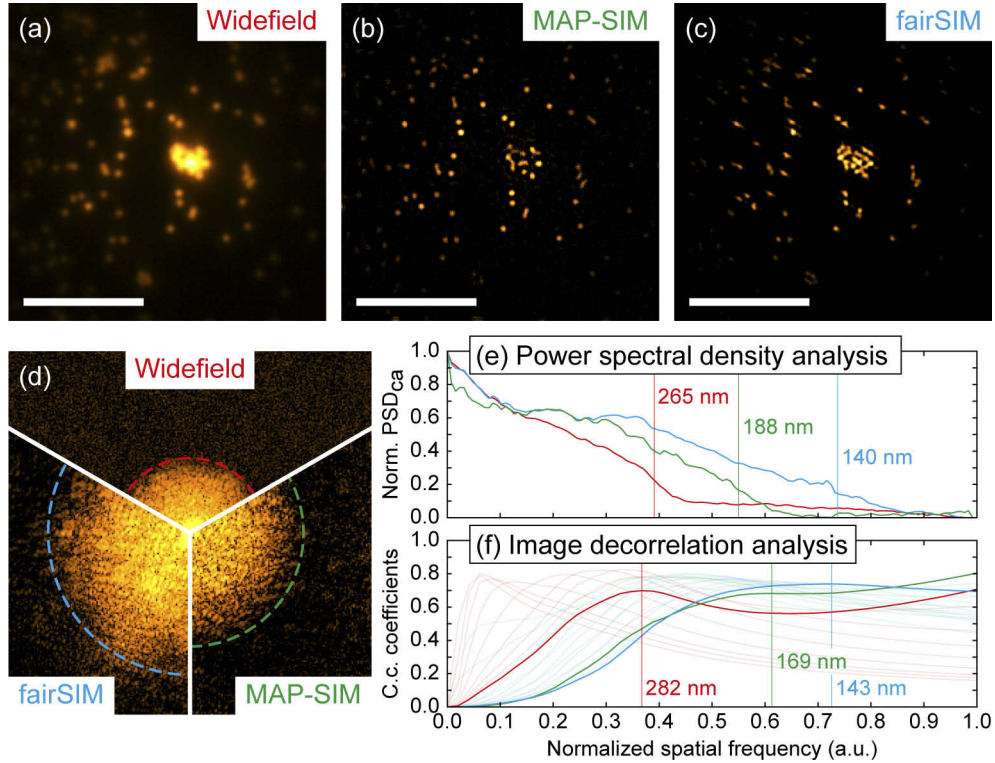


Fig. 7. Measurements of the spatial resolution of widefield and SR-SIM images. (a)-(c) A $13.25 \mu\text{m} \times 13.25 \mu\text{m}$ FOV of the widefield, MAP-SIM and fairSIM reconstructed images, respectively. (e)-(f) Determination of the global spatial resolution in image data using power spectral density analysis (PSD_{ca} [25,26]) and image decorrelation analysis (imDecorr [27]). (d) Sections of the 2D Fourier transform of the images (a)-(c). The resolution limit of each imaging technique was determined with PSD_{ca} and the decorrelation method ((e) and (f)). The spatial frequency axes are normalized by the sampling rate $f_s = 1/(2 \cdot pps) = 9.66 \mu\text{m}^{-1}$, where $pps = 51.75 \text{ nm}$ is a projected pixel size given by the physical size of the pixels on the camera sensor ($3.45 \mu\text{m}$) and the magnification of the objective lens in combination with the tube lens ($66.666\times$). All resolution assessing methods indicate an improvement in the reconstructed SR-SIM images by almost a factor of 2. Scale bars are $5 \mu\text{m}$.

4. Conclusion

In this paper, we have demonstrated a novel approach for 2-beam structured illumination microscopy using an all-fiber optical implementation. The highly compact design and flexibility of this SR-SIM device, while also maintaining the robustness required for interferometry were achieved by using a microelectromechanical systems (MEMS) based fiber switch for rapid pattern angle switching in combination with 1×2 fiber splitters and a piezoelectric crystal for pattern phase shifting. By proper selection of the telescope magnification, the pattern period can be flexibly adjusted from a coarse interference pattern up to the highest possible pattern frequency. As a proof-of-concept, we have demonstrated this for a single pattern frequency by utilizing very cost-effective components, such as an industry-grade CMOS camera, which currently also

limits the maximum frame rate of the system. Furthermore, the fiber optics-based approach allows for the rather straight-forward realization of multi-color SIM imaging in the future. Our fiberSIM device provides very promising preliminary imaging results indicating that this could become the basis of a versatile “Plug&Play” illumination module with the capability of turning any conventional microscope body into a SR-SIM microscope.

Funding. Universitätsbibliothek Bielefeld (Open Access Publication Fund); European Regional Development Fund (Fiber-SIM); Horizon 2020 Framework Programme (766181); Deutsche Forschungsgemeinschaft (415832635); České Vysoké Učení Technické v Praze (SGS20/179/OHK3/3T/13).

Acknowledgments. The authors would like to thank Jochen Linnenbrügger for his help with designing the hexagonal fiber collimator assembly and Henning Ortkraß for productive discussion and assistance during the system speed performance evaluation. Funding for this project was provided by the European Regional Development Fund 2014 - 2020 programme “NRW-patent validation” under the project “Fiber-SIM”. This project has also received funding from the European Union’s Horizon 2020 research and innovation program under the Marie Skłodowska-Curie Grant Agreement No. 766181, project “DeLIVER” and by the Grant Agency of the Czech Technical University in Prague within the grant No. SGS20/179/OHK3/3T/13 “Modern Optical Imaging Systems with Non-linear Point Spread Function and Advanced Algorithms for Image Data Processing”. TH acknowledges funding by the Deutsche Forschungsgemeinschaft (DFG, German Science Foundation) under project number 415832635. We acknowledge support for publication costs by the Open Access Publication Fund of Bielefeld University.

Disclosures. TH and GW submitted a patent application related to fiberSIM through their employer (Bielefeld University). The other authors declare no conflicts of interest.

References

1. M. G. L. Gustafsson, “Surpassing the lateral resolution limit by a factor of two using structured illumination microscopy,” *J. Microsc.* **198**(2), 82–87 (2000).
2. M. G. L. Gustafsson, L. Shao, P. M. Carlton, C. J. R. Wang, I. N. Golubovskaya, W. Z. Cande, D. A. Agard, and J. W. Sedat, “Three-dimensional resolution doubling in wide-field fluorescence microscopy by structured illumination,” *Biophys. J.* **94**(12), 4957–4970 (2008).
3. P. Kner, B. B. Chhun, E. R. Griffis, L. Winoto, and M. G. L. Gustafsson, “Super-resolution video microscopy of live cells by structured illumination,” *Nat. Methods* **6**(5), 339–342 (2009).
4. R. Heintzmann and T. Huser, “Super-Resolution Structured Illumination Microscopy,” *Chem. Rev.* **117**(23), 13890–13908 (2017).
5. A. Markwirth, M. Lachetta, V. Mönkemöller, R. Heintzmann, W. Hübner, T. Huser, and M. Müller, “Video-rate multi-color structured illumination microscopy with simultaneous real-time reconstruction,” *Nat. Commun.* **10**(1), 4315 (2019).
6. P. Křížek and G. M. Hagen, “Spatial light modulators in fluorescence microscopy,” in *Microscopy: Science, Technology, Applications and Education A*. Méndez-Vilas and J. Díaz, eds. (Formatex, 2010), chap. Spatial li, pp. 1366–1377, microscopy ed.
7. P. Křížek, I. Raška, and G. M. Hagen, “Flexible structured illumination microscope with a programmable illumination array,” *Opt. Express* **20**(22), 24585–24599 (2012).
8. J. T. Frohn, H. F. Knapp, and A. Stemmer, “True optical resolution beyond the Rayleigh limit achieved by standing wave illumination,” *Proc. Natl. Acad. Sci.* **97**(13), 7232–7236 (2000).
9. M. Brunstein, K. Wicker, K. Hérault, R. Heintzmann, and M. Oheim, “Full-field dual-color 100-nm super-resolution imaging reveals organization and dynamics of mitochondrial and ER networks,” *Opt. Express* **21**(22), 26162–26173 (2013).
10. J. Cossen, T. Hinsdale, R. Ø. Thorsen, M. Siemons, F. Schueder, R. Jungmann, C. S. Smith, B. Rieger, and S. Stallinga, “Localization microscopy at doubled precision with patterned illumination,” *Nat. Methods* **17**(1), 59–63 (2020).
11. J. Roth, J. Mehl, and A. Rohrbach, “Fast TIRF-SIM imaging of dynamic, low-fluorescent biological samples,” *Biomed. Opt. Express* **11**(7), 4008 (2020).
12. B. Hyle Park, M. C. Pierce, B. Cense, S.-h. Yun, M. Mujat, G. J. Tearney, B. E. Bouma, and J. F. d. Boer, “Real-time fiber-based multi-functional spectral-domain optical coherence tomography at 1.3 μm ,” *Opt. Express* **13**(11), 3931–3944 (2005).
13. S. Coquoz, A. Bouwens, P. J. Marchand, J. Extermann, and T. Lasser, “Interferometric synthetic aperture microscopy for extended focus optical coherence microscopy,” *Opt. Express* **25**(24), 30807–30819 (2017).
14. E. Chung, D. Kim, and P. T. So, “Extended resolution wide-field optical imaging: objective-launched standing-wave total internal reflection fluorescence microscopy,” *Opt. Lett.* **31**(7), 945–947 (2006).
15. B.-J. Chang, V. D. Perez Meza, and E. H. K. Stelzer, “csiLSFM combines light-sheet fluorescence microscopy and coherent structured illumination for a lateral resolution below 100 nm,” *Proc. Natl. Acad. Sci. U. S. A.* **114**(19), 4869–4874 (2017).
16. H. W. Lu-Walther, M. Kielhorn, R. Förster, A. Jost, K. Wicker, and R. Heintzmann, “fastSIM: A practical implementation of fast structured illumination microscopy,” *Methods Appl. Fluoresc.* **3**(1), 014001 (2015).

17. A. Sandmeyer, M. Lachetta, H. Sandmeyer, W. Hübner, T. Huser, and M. Müller, “DMD-based super-resolution structured illumination microscopy visualizes live cell dynamics at high speed and low cost,” *bioRxiv* pp. 1–32 (2019).
18. R. Fiolka, M. Beck, and A. Stemmer, “Structured illumination in total internal reflection fluorescence microscopy using a spatial light modulator,” *Opt. Lett.* **33**(14), 1629–1631 (2008).
19. M. Müller, V. Mönkemöller, S. Hennig, W. Hübner, and T. Huser, “Open-source image reconstruction of super-resolution structured illumination microscopy data in ImageJ,” *Nat. Commun.* **7**(1), 10980 (2016).
20. T. Lukeš, P. Křížek, Z. Švindrych, J. Benda, M. Ovesný, K. Fliegel, M. Klíma, and G. M. Hagen, “Three-dimensional super-resolution structured illumination microscopy with maximum a posteriori probability image estimation,” *Opt. Express* **22**(24), 29805–29817 (2014).
21. P. Křížek, T. Lukeš, M. Ovesný, K. Fliegel, and G. M. Hagen, “SIMToolbox: A MATLAB toolbox for structured illumination fluorescence microscopy,” *Bioinformatics* **32**(2), 318–320 (2016).
22. K. Wicker, “Non-iterative determination of pattern phase in structured illumination microscopy using auto-correlations in Fourier space,” *Opt. Express* **21**(21), 24692–24701 (2013).
23. K. Wicker, O. Mandula, G. Best, R. Fiolka, and R. Heintzmann, “Phase optimisation for structured illumination microscopy,” *Opt. Express* **21**(2), 2032–2049 (2013).
24. Y. Guo, D. Li, S. Zhang, Y. Yang, J.-J. Liu, X. Wang, C. Liu, D. E. Milkie, R. P. Moore, U. S. Tulu, D. P. Kiehart, J. Hu, J. Lippincott-Schwartz, E. Betzig, and D. Li, “Visualizing Intracellular Organelle and Cytoskeletal Interactions at Nanoscale Resolution on Millisecond Timescales,” *Cell* **175**(5), 1430–1442.e17 (2018).
25. J. Pospíšil, K. Fliegel, and M. Klíma, “Assessing resolution in live cell structured illumination microscopy,” in *Photonics, Devices, and Systems VII*, vol. 10603, K. Fliegel and P. Páta, eds. (SPIE, Prague, Czech Republic, 2017), vol. 10603, pp. 1–7.
26. J. Pospíšil, T. Lukeš, J. Bendesky, K. Fliegel, K. Spendier, and G. M. Hagen, “Imaging tissues and cells beyond the diffraction limit with structured illumination microscopy and Bayesian image reconstruction,” *GigaScience* **8**(1), 1–12 (2019).
27. A. Descloux, K. S. Grußmayer, and A. Radenovic, “Parameter-free image resolution estimation based on decorrelation analysis,” *Nat. Methods* **16**(9), 918–924 (2019).